Aerodynamic Characteristics of a Highly Swept Wing in Steady/Unsteady Pitching States and Effects of Flap Control at Large Incidence*

Ting-Ding Hsing
Beijing University of Aeronautics and Astronautics, Beijing 100083, P.R.China

Guang-Zhi Yu Zhi-Fu Gu
Peking University, Beijing 100871, P.R.China

Abstract

Experiments were conducted to investigate the aerodynamic characteristics of a 74° swept delta-wing model equipped with an apex-flap and leading-edge vortex-flaps for the study of steady state with the angle of attack varying from 0° to 90° and for the unsteady pitching state with the frequencies 0.4 ,0.8 and 1.2 Hz. The corresponding "nondimensional pitch rate" parameters K were to vary from 0.02 to 0.15, which are typical of airplane maneuvers. These tests were conducted in a low-speed wind tunnel of 2.25m in diameter with Reynolds number ca. 1×10^6 , supplemented by colored water visualizations conducted in a $0.4m \times 0.4m$ water channel. The relations of the static aerodynamic coefficients varying with the angle of attack are analyzed according to the flow phenomena which are different in three zones of angle of attack. The dynamic hysteresis of the aerodynamic loads in unsteady state and the effects of deflecting flaps on the vortex control are discussed. Comparisons between the results of experiment and computation by solving the Navier-Stokes equations are made. The unsteady pitching motion of the model causes the hysteretic variation of the aerodynamic coefficients but can still keep the advantageous effects of flap on vortex control as in the steady state. The fact that part of the results of the calibration test of a basic delta wing with no flaps are in agreement with the corresponding values found in references may enhance the reliability of the present tests.

Nomenclature

Cr	Root chord
S	Wing area
Sf	Area of AF
Sv	Area of LEVF
AF	Apex flap
LEVF	Leading-edge vortex-flap
LE	Leading edge
b_a	Aerodynamic chord
l	Wing span
V_∞	Velocity of the free stream
p	Pressure
q_∞	Free stream dynamic pressure
t	Time
CL	Lift coefficient
Cd	Drag coefficient
Cn	Normal force coefficient
Ca	Axial force coefficient
Cm	Pitching moment coefficient
Cm_r	Rolling moment coefficient
Ck	CL/Cd, Lift-drag ratio, aerodynamic efficiency
x	Cartesian x-coordinate
y	Cartesian y-coordinate
z	Cartesian z-coordinate
Re	Reynolds number $Re = V_\infty b_a/\nu$
α	Angle of attack, incidence
α_{ad}	Angle of attack where hysteretic loop ends
δf	Deflection angle of AF
δv	Deflection angle of LEVF
	Pitching angular velocity
β	Coefficient of artificial compressibility

Subscripts

0	Initial condition
cr	Critical condition
min	Minimum
max	Maximum
∞	Free stream

Introduction

As the current operational fighters have experienced the angle of attack over- shooting 60° in maneuvers at combat[1], the next generation of aircraft being considered is to fly at angles of attack far over its critical value which is in general 25° to 35°. It is well known that the flow over a delta-wing at constant angle of attack is dominated by two large bounded vortices that result from the flow separation at the leading edge. However the vortices will break down causing the passing flow unsteady when the angle of attack increases approaching a critical angle. There are many unanswered problems on the behavior of the wing not

* The project supported by National Natural Science Foundation of China

only in steady state but also in unsteady state after the vortex breakdown and the ways suitable for controlling the development of vortices. These problems have led us to a growing interest in the investigation of the aerodynamic characteristics of highly swept wings at very high angle of attack as well as the control of vortical flow. There need both an increase in the physical insight and an improvement of the understanding of all relevant phenomena. For several years the first author had led investigations[2,3,4] to find ways that can avoid the decrease of lift and can increase further the aerodynamic efficiency of a highly swept (74°) delta wing equipped with vortex flaps. It was found in the investigation that if the forepart of the delta wing called apex flap deflectable about a transverse axis is to droop down, then the vortices separated from the apex flap and the leading-edge vortex flaps will interact to yield a higher lift and larger lift-drag ratio than that produced by a wing without an apex flap. These previous investigations were carried out for steady states with the angle of attack less than 35°. Based on this background the objectives of the present test program were plotted to involve the study of steady state with the angle of attack varying from 0° to 90°. and the unsteady state caused by a sinusoidal pitching motion of the wing under an excursion of angle of attack between 0° and 73° .

Experimental model, setup and test procedure

The planform of the present model and the installation of the apex-flap(AF) and leading-edge vortex-flaps(LEVF) are as shown in Fig.1(a) with its geometrical data listed in table 1. This model is modified from that used in the former investigations (Fig.1(b)). The difference is in that the LEVF of the present model are located out of the main delta part instead of within it. In the previous case the leading edge of the LEVF is in alignment with that of the AF, therefore the LEVF are to occupy the limited wing space. The relative areas of the present AF and LEVF with respect to the whole wing area are 5.65% and 25.7% respectively. The AF and LEVF can be deflected up and down about hinges at their trailing lines with respect to the main delta wing. In the tests, the AF was deflected to $-15°, 0°$ and 15°. and the deflections of LEVF were $-30°, 0°$ and 30°. (negative means to droop down). The model used for wind tunnel tests was made of 6mm thick aluminum plate with the leading edge (LE) sharpened by an upward cut from the lower surface to fix the flow separation there but the trailing edge was blunted. The thickness of LEVF is 1mm which is relatively thin and can be treated as zero in computation. The model was mounted on a sting-type six-component strain gauge balance (Fig.2) connected to a frame which can be rotated to vary the angle of attack from -4° to 90°. in the present tests. The origin of the Cartesian coordinates system was located on the aerodynamic center of the wing with the x-axis set in the direction of oncoming flow and the y-axis directing upward. The model for flow visualization in water channel was made of plastics and had its size 1/3 of the model used for wind tunnel test. The low speed wind tunnel of the Peking University has a circular test section of 2.25m in diameter with Reynolds number 2×10^6 to 2.7×10^6 per meter for wind speed of 30 m/sec to 40 m/sec respectively. The water channel of the Beijing University of Aeronautics and Astronautics has a 0.4m x 0.4m square test section with a Reynolds number of $7x10^3$ at flow speed 4cm/sec. In steady state tests, the angle of attack varied from -4° to 90° with data points recorded at intervals of 2° for $\alpha = -4°$ to 10° and 5° for α above 10°. In the unsteady state with the model in pitching, three cases of α excursion i.e. $0° \rightleftharpoons 40°, 20° \rightleftharpoons 60°$ and $0° \rightleftharpoons 73°$ were adopted for purpose of looking changes with the change of amplitude. The sinusoidal pitching motion were proceeded according to the rule of $\alpha = \alpha_0 + (\alpha_{max} - \alpha_0) sin\omega t$, in which ω is the angular velocity. In wind tunnel tests, the adopted pitching frequencies were 0.4, 0.8 and 1.2 Hz. Correspondingly the reduced frequencies were k= 0.03, 0.06 and 0.12 with the nondimensional pitch rate K varied from 0.02 to 0.15. These values are typical and comparable to those happened in maneuvers. For the flow visualization tests held in the water channel, it was to keep $V_\infty = 4cm/sec$ with the Re=$7x10^3$ and the pitching frequencies 0.012 to 0.06 Hz corresponding to k=0.2 to 1.0 and K=0.3 to 1.5 respectively. The visualization records were employed for assessing the influence of various flow parameters. In wind tunnel tests, the pitching motion was actuated by a computer controlled D.C.motor. The analog signals sent by the balance, pressure transducers, etc. were prefiltered by using an analog low pass filter with 30 Hz cutoff frequency. Electronic coordination between data acquisition system and apparatus control system was used to allow efficient operation and sychroneous collection of electrical signals. During data collection, signals of 120 points were drawn in a sample for every cycle of vibration and 10 samples were taken to make an average value for every point i.e. for every angle of attack. After the data were converted and corrected for balance interactions etc. the structural modes of vibration were to be filtered out by a low pass filter with 17 cut-off frequency. The aerodynamic forces and moments were extracted to calculate the aerodynamic coefficients after the static data from wind-off runs were subtracted from the wind-on data. Finally, results of the force measurements were plotted in form of coefficients including the coefficient of normal force Cn, axial force Ca, lift force CL, drag force Cd, pitching moment Cmz and the aerodynamic efficiency Ck=CL/Cd vs. the angle of attack.

Steady Aerodynamic Characteristics

The experimental results show that the variation of the static aerodynamic behavior is quite different in three regions of angle of attack, therefore the steady aerodynamic characteristics may be discussed as follows:

(1) The first region, $0° < \alpha < 30°$

In this region , the flow over the wing is basically dominated by the two primary bounded vortices separated from the leading-edge of the flaps as shown by the visualization results (for α below 5° the influence is small). In company with the increase of the angle of attack, these vortices move inboard and grow in size. They become stronger and their influence on the total forces and moments grows till the breakdown of the vortices merges as the α approaches to 30°. However the breakdown of vortices can be delayed when the AF droops down ($\delta_f < 0°$) and vice versa if AF tips up ($\delta_f > 0°$) as can be seen in the flow visualization. Taking the pictures of Fig.3(a) and Fig.3(b) for example, they display the patterns of flow around the model for $\delta_v = 30°, \delta_f = 5°$ and -15° respectively at $\alpha = 30°$. It can be seen that at $\delta_f = 5°$ the bounded vortex suddenly expands over the aft part of the wing indicating the happening of vortex breakdown which however doesn't appear at $\delta_f = -15°$. Therefore it is clear that the delay of vortex breakdown is contributed by the action of drooping down the AF.This happens also in other cases of δ_v deflection.In addition, as AF droops down,the AF vortices will move toward LEVF to merge with the LEVF vortices after leaving AF, which will strengthen the negative pressure acting on LEAF and in turn to reduce the drag because of increase of the thrustwise axial force in forward direction. It is well known that the advantage of employing vortex flap on wing to produce thrustwise force component is effective on reducing the drag and increasing the lift-drag ratio at a cost of slight lift reduction[5,6]. Nevertheless to droop AF down will enhance the advantageous function of LEVF but with less lift loss. In contrast, if$\delta_v > 0°$ i.e. to tip LEVF up, the thrustwise force will reverse its direction to produce drag. The other result of drooping AF down ($\delta_f < 0°$) is the reduction of adverse pressure gradient along the streamline, which is conducive to delay of vortex breakdown and to increase of C_{Lmax} as well as the critical angle of attack α_{cr}. In other words, the phenomenon of vortex breakdown emerges earlier at $\delta_f > 0°$ than at $\delta_f < 0°$. Many experiments and computations show that the weaker vortex will be drawn toward the stronger vortex rotating in same sense and merging together, if the distance between them are smaller than a certain critical value. For this reason, the LEVF of present model was designed to tape at its front part for sake of diminishing the interval between the cores of the two vortices. Flow visualization(Fig.3(b)) has verified the concept that the separated vortices of AF and LEVF merged earlier as the vortex of AF became weaker when AF drooped down. Correspondingly,the force measurements can verify that the coefficient of axial force Ca decreases more negatively with the increase of α by deflecting AF downward(Fig.4(b)), while it can keep the curve of normal force coefficient Cn vs. α nearly unchanged (Fig.4(a)). As a result, the curves of lift coefficient CL vs. α , drag coefficient Cd vs. α and the polar curve CL vs. Cd will be of the form as shown in Fig.4(c),Fig.4(d) and Fig.4(e) respectively because of existing the relationship: $C_d = C_a cos(\alpha) + C_n sin(\alpha)$, and $C_L = C_n cos(\alpha) - C_a sin(\alpha)$.

(2) The second region, $30° < \alpha < 55°$

In this range, following the movement of breakdown point from the trailing edge to the tip, the flow field gradually becomes disordered as can be seen by comparing the visualization pictures for $\alpha = 30°$ and 45° (Fig.3(c) and Fig.3(d)). The effects of disordered flow field are to be reflected on the aerodynamic characteristics such that the positive gradients of the Cn and CL vs. α curves will gradually become negative after $\alpha = 35°$. Moreover, the down droop of AF will cause the Cn_{max}, CL_{max} and α_{cr} to increase and the Ca to decrease further because of the delayed breakdown of vortices.

(3) The third region, $55° < \alpha < 90°$

In this region the stable vortices disappear completely and the flow becomes like wake-type and unsteady, which causes the aerodynamic forces acting on the wing nearly unchanged with the change of angle of attack, therefore the variation of Cn and Ca are only slight with the increase of α till the CL and Cd approach to the value of -Ca and Cn at $\alpha = 90°$ (Fig.4). In accordance with that,the result is to cause the CL/Cd curve less effected by the deflection of δ_f and nearly perpendicular to the Cd axis (Fig.4(e)). As to the variation of pitching moment coefficient Cm vs.α, the tendency is similar to that of the Cn vs.α throughout the whole 3 regions.

Unsteady Aerodynamic Characteristics

The experimental study of the unsteady aerodynamic characteristics of the pitching wing was conducted for three ranges ofα excursion. They are $0° \rightleftharpoons 40°$ for low to moderate α, $20° \rightleftharpoons 60°$ for middle α and $0° \rightleftharpoons 73°$ for low to very high α. Correspondingly the amplitudes are 40°, 40° , and 73° respectively. Samples of Cn and Ca vs. α are presented in Fig.6,in which

curves related to k= 0.03, 0.06 and 0.09 are drawn and for each k three curves corresponding to 4 K-values are illustrated. The curves of Cm vs. α for k=0.03 are drawn in Fig.7. It is worth to note that for a definite k, larger K means having larger amplitude. Taking the Fig.6 which is drawn for $\delta_v = -30°$. and $\delta_f = -15°$ for example, the curves of Cn vs. α (Fig.6(a)) show that Cn has an increment ($\Delta Cn > 0$) at pitching-up and a decrement ($\Delta Cn < 0$) at pitching-down forming a hysteretic loop to enclose the static Cn vs. α curve (K=0) in. The loop looks like a leaf with its maximum height diminishing as k increasing from 0.03 to 0.09. The pitching motion is to enhance the α_{cr}, Cn_{max} and the CL_{max} also. This phenomena appear in the Cn vs. α curves for the α excursions not only in $0° \rightleftharpoons 40°$. but also in $20° \rightleftharpoons 60°$ and $0° \rightleftharpoons 73°$. It is apparent that for a definite k, the hysteretic loop expands with the increase of amplitude or K such that the loop of larger K is to enclose the loop of smaller K, which results in increase of Cnmax and the slope of Cn vs. α at pitching-down. In table 2 and table 3, there are data of α_{cr}, Cn_{max} and α_{ad} corresponding to various k and K for the basic delta model with and without flaps respectively. These data show straightforward the advantageous tendency of the variation of aerodynamic behavior. The reason behind that is the breakdown is delayed at pitching-up, which can cause the increment of α_{cr} even to 20 deg. as K increases. The angle α_{ad} is the angle of attack at which the loop ends or the pitching-up branch coincides with the pitching-down branch. When α reduces to α_{ad} during pitching-down, the pattern of flow dominated by the bounded prime vortices recovers and the wake-type flow disappears. Moreover, α_{ad} is to decrease with the increase of K. In addition, as α approaching to α_{ad} in pitching-down motion a small peak appears, which indicates that one bounded vortex has rebuilt before the other one rebuilt at $\alpha = \alpha_{ad}$. The feature of unsteady characteristic curves of axial force coefficient Ca vs.α (Fig.6(b)) is first that the Ca curve with larger K will enclose that of smaller K but the increment $\Delta Ca < 0$ is for pitching-up and $\Delta Ca > 0$ for pitching-down with its form looking like a piece of slender leaf. The second feature is that the hysteretic phenomenon is less prominent at the first region ($0° < \alpha < 30°$) than that at the 2nd and 3rd region , because in the latter two regions the flow fields are gradually dominated by that of wake type. The last feature is that the minimum Ca is to appear at larger α where the gradient changes its sign for larger amplitude or larger K. Moreover the absolute value $|Ca_{min}|$ is to decrease with the increase of δ_v and δ_f. The hysteretic phenomenon appears also in the curve of pitching moment coefficient Cm vs.α , as can be seen for example from the curves of $\delta_v = -30°$and$\delta_f = -15°$ in Fig.7. The characteristic Cm curves show that in the 2nd and 3rd region, the hysteretic region grows with the increase of K, which differs somewhat from that of the Cn vs. α curves. The variation of the unsteady CL and Cd vs. α is similar to that of Cn and Ca vs. α since CL and Cd are in function of Cn and Ca (Fig.8).

Flap Aerodynamic Control

In the steady state the strength of the bounded vortices will be greater for $\delta_v > 0°$ than $\delta_v < 0°$ because the bounded vortices are at places nearer to the LEVF as can be seen in the visualization pictures(Fig.3), and the local angle of attack is higher there than in the case of $\delta_v < 0$. These may the reason that the updeflection of LEVF($\delta_v > 0°$) will enhance Cn and CL as well as Ca and Cd as compared to the case of downward deflected LEVF($\delta_v < 0°$). Based on the above explained action of the δ_v along with the effect of δ_f discussed in the previous paragraphs, the effective contribution of using AF and LEVF to the wing aerodynamic characteristics can be summarized(refer to Fig.4 and Fig.5) as follows:

(1) In the first region, increasing δ_v will cause Cn and CL as well as Ca and Cd to increase. However increasing δ_f causes only a little increase of CL and Cd compared with that of decreasing δ_f. (2) In the second region, increasing δ_v will cause Cn_{max} and CL_{max} to decrease and Ca to increase. Corresponding to the decrease of Cn, Cd will decrease also. The CL_{max} and α_{cr} are higher for $\delta_f < 0°$ than that for $\delta_f > 0°$. The tendency that CL and Cd are smaller at $\delta_v > 0°$ than at $\delta_v < 0°$ will continue on in the third region. (3) In the third region, increasingδ_f will cause a little decrease of CL and Cd compared with that of decreasing δ_f. Throughout the regions from $\alpha = 0° to 90°$, the polar curve CL vs. Cd for $\delta_v > 0°$ at definite δ_f shrinks to locate within that corresponding to $\delta_v < 0°$. The distance between these two curves becomes larger in the third zone than in other zones (Fig.5(e). However, for definite δ_v, the interval between polars for $\delta_f > 0°$ and $\delta_f < 0°$ at the third zone is trivial(Fig.4(e)), which indicates that the effect of deflecting δ_f has lost in this region. Reducing δ_v and δ_f will cause the lift-drag ratio CL/Cd to increase in the 1st region, although the variation of δ_v is less effective than δ_f. The data of aerodynamic coefficients CL and Cd corresponding to $\alpha = 15°, 65°$ and $90°$. representing the flow in 1st,2nd and 3rd region respectively are listed in table 4 for the cases of$\delta_v = -50°$,$50°$ and$\delta_f = -20°$. The data of CL and Cd related to the case of $\delta_f = -15°$ and $15°$ and $\delta_v = -30°$ listed in table 5 together with the data listed in table 4 are both conducive to confirmation of the effects of AF and LEVF control as described above. The data for unsteady pitching motion as listed in table 2 and 3 indicate that the present model with flaps has α_{cr} ca. $3°$. greater than that of the pure delta wing($\delta_f = 0$) besides having little decrease of Cnmax

and with smaller axial force. These results can illuminate the advantages of employing AF and LEVF flaps on the control of vortical flow around highly swept wing at large incidence both in steady and unsteady cases. It seems that the knowledge of flap control in steady state is worthy for the prediction of the effect of flap control in unsteady state.

Comparison of Experimental and Computational Results

For the convenience of making comparison between the experimental and computational results, the model supporter was modified to locate symmetrically with respect to the wing plane at near the trailing edge than beneath the wing. Experiments were conducted for this modified model and the results are drawn in parallel with the computational values as shown in Fig.9. The computational results were obtained by solving the 3-D Navier-Stokes equations for incompressible flow by the pseudo-compressibility method. In this method an item $\beta\partial p/\partial t$ was added in the continuity equation, where β is a constant, p and t are pressure and time respectively. In the computation[7] an approximately factorized implicit scheme of Beam-Warming type was used. Artificial viscosity of O(0.1) was employed to keep the computation stable because of using 2nd order central difference scheme. However comparison was made with respect to the results got by using the 3rd order upwind compact difference scheme which needs no artificial viscosity in computation. No apparent difference between them had been found. In the Fig.9, apparent difference between the experimental and computational Cn and Ca vs. α curves can be found in the region ofα = 20° to 40°. The reasons concerned may be that the computational $Re = 10^4$ is much smaller than the $Re = 10^6$ in the experiments and no consideration concerning the turbulence have yet been taken. However the agreement of computational and experimental CL/Cd curves seems satisfactory. All of them have confirmed the advantage of using flaps to control the vortex flow because of having the effect of reducing the drag and increasing the CLmax and α_{cr} etc. by drooping down the AF as found in the experiments with their explanation given above.

Accuracy of Experiments

The accuracy of the experiments was verified through testing a calibration delta-wing model with 74° swept angle which is same as that of the original main part of the flapped wing model. The aspect ratio of the calibration delta-wing is λ=1.135. The CL-α and Cd-α curves for the calibration model are as shown in Fig.10. Generally the curves for $\delta_f = 0°$ should pass through the origin point at $\alpha = 0$ in steady state, because the model is symmetrical with respect to the wing plane. Nevertheless there is a small deviation of 0.002 which is however merely 0.15% and 0.11% in error relative to the CLmax and Cdmax respectively and is permissible to be neglected. The gradient of CL -α curve for $\alpha < 5°$. is 0.022 per degree which agrees with the corresponding value found in the reference [8]. For $\alpha > 5°$, the gradient $\frac{dCL}{d\alpha}$ increases because of the appearance of the bounded vortices which will reduce the viscous lift as generally called. The $CL_{max} = 1.3$ at α_{cr} is a little greater than the average $CL_{max} = 1.2$ for $\lambda = 1.15$ delta wing at $Re = 1 \times 10^6$ as found in the reference, in which $C_L = 1.3$ is for λ=1.5 delta wing. According to the statistics, CL_{max}=1.3 is on the upper bound. However $\alpha_{cr} = 34°$ is well in agreement with the statistical value of 35° for $\lambda < 1.2$. For the case of $\alpha > \alpha_{cr}$, the Cn is 1.28 for$\alpha = 65°$. and 1.19 for $\alpha = 90°$ which are quite fit with the 1.22 and 1.06 for $\alpha = 65°$ and 90°. respectively at$\lambda = 1.0$ as found in the literature although being a little greater. For the unsteady state, the data listed in table 6 are Cn_{max}, α_{cr} and α_{ad} as well as the corresponding data found in reference [9] for λ=1 delta wing. It is apparent through comparison that the values of the calibration Cnmax are somewhat greater for all K, which is reasonable if the Reynolds no.effects is considered, since the calibration $Re = 1 \times 10^6$ is greater than the $Re = 4.5 \times 10^5$ found in the reference. The disagreement of some α_{ad} to their counterparts in the reference is related to the difference of their amplitude of angle of attack during pitching motion. The comparison has shown the degree of accuracy and the reliability of the present investigation.

Conclusions

Experiments including the flow visualization and force measurement for steady flow and unsteady flow around a pitching 74° swept delta-wing model with flaps were conducted. Comparison between the experimental and computational results based on solving Navier-Stokes equations was made. The aerodynamic behavior of the present flapped delta wing and the effects of flap control can be summarized as follows:

1. The variation of aerodynamic characteristics with the increase of angle of attack can be divided into three regions i.e.α = 0° to 30°, 30° to 55° and 55° to 90° according to the flow phenomena dominated by leading-edge vortices, vortex breakdown and wake type flow respectively.

2. By the increase of LEVF deflection, CL and Cn increase apparently and Ca increases too in the range α = 0° to 30°, while CL and Cn decrease in the range α = 50° to 90°. CLmax,Cnmax and α_{cr} decrease with

the increase of LEVF.

3. By the decrease of LEVF deflection, Ca decreases apparently while CL_{max}, Cn_{max} and α_{cr} increase. However the effect of flap deflection on CL and Cn is slight in the ranges of $\alpha = 0°$ to 30°. and $\alpha = 55°$ to 90°

4. For the CL vs. Cd curves, the effect of drooping down the AF is to increase the value of $(CL/Cd)_{max}$ in the range of $\alpha = 0°$ to 30°. But the effect of AF control is trivial in the range of$\alpha = 55$ to 90°, however can use the LEVF instead of using the AF for more effective control in this range.

5. Following the variation of angle of attack from increase to decrease, the aerodynamic hysteresis behavior of all coefficients appear in the unsteady state during the sinusoidal pitching of the model. The hysteretic region of the coefficients like CL,Cn,Cd and Ca are deformed to be more slender as the reduced frequency k increases, while for a definite k the area of hysteretic region expands as the nondimensional pitch rate K increases.

6. The agreement between the calibration testing data of the delta-wing model and the corresponding data found in the literature is conducive to confirmation of the reliability of the present experimental results.

References

1. Lerner, Eric J., First international X-plane to fly, Aerospace America, 1987,8.
2. Hsing,T.D., Gao,W.H., et al., Effectiveness of combination of apex-flap and leading-edge vortex-flaps on a 74° swept delta-wing, Paper ICAS-88-4.5.1, Israel, Sept.1988.
3. Hsing,T.D., Zhang,Z.Q.,et al., A study of the interaction of separated vortices in transonic and supersonic flow on improving the aerodynamic characteristics of vortex-flap, IUTAM Symposium in Novosibirsk/USSR, Springer-Verlag, pp.475-483,1990.
4. Hsing,T.D., Zhang,Z.Q., Zhuang,F.G., The impact of apex-flap on vortex-flapped delta and double delta wings, AIAA-91-3218,1991.
5. Lamar,J.G. et al., Development of a vortex-lift design procedure and application to slender maneuver wing configuration. J.Aircraft,1981, 18(4), 259-266.
6. Rao,D.M., Leading-edge vortex-flap experiments on a 74° delta wing, NASA CR-159161, 1979,11.
7. Yuan, L.,Hsing, T.D., A comparison of the experimental and computational study on the effects of vortex-control by deflecting flaps on a highly swept delta wing, 1st International Conference on Advances in Fluid Mechanics, New Orleans USA, 1996,6 (accepted,to appear).
8. Schlichting/Truckenbrudt, Aerodynamik des Flugzeuges, Zweiter Band, Springer-Verlag,Seite 71 und 122, 1959.
9. Mohammad-Ameen M. Jarrah, Low-speed wind-tunnel investigation of flow about delta wings oscillating in pitch to very high angle of attack. AIAA P-89-0295, 1989.

Tables

Table 1. Geometrical parameters of wings (length unit: meter)

kind of model	root chord	mean aerodymic chord	wing area	aspect ratio	span	area ratio AF to wing	area ratio LEVF to wing
delta-model	0.590	0.393	0.10	1.153	0.34	7.35 %	—
delta-model with flaps	0.590	0.380	0.13	1.623	0.46	5.65 %	25.7%

Table 2. Unsteady aerodynamic characteristic data of the calibration delta model ($\delta_f = 0°$)

k	α	$0° - 90°$	$0° - 40°$	$20° - 60°$	$0° - 73°$
0.03	K	0	0.02	0.04	0.06
	α_{ad}			26°	17°
	α_{cr}	34°	39°	46°	50°
	Cn_{max}	1.50	1.85	2.00	2.05
0.06	K	0	0.03	0.06	0.09
	α_{ad}			22°	16°
	α_{cr}	34°	42°	51°	55°
	Cn_{max}	1.50	1.85	2.10	2.15
0.09	K	0	0.04	0.08	0.12
	α_{ad}		24°	20°	12°
	α_{cr}	34°	41°	53°	60°
	Cn_{max}	1.50	1.85	2.10	2.20

Table 3. Unsteady aerodynamic characteristic data of the experimental model with $\delta_v = -30°, \delta_f = -15°$

k	α	$0° - 90°$	$0° - 40°$	$20° - 60°$	$0° - 73°$
0.03	K	0	0.02	0.04	0.06
	α_{cr}	38°	42°	48°	54°
	Cn_{max}	1.50	1.80	1.92	2.03
0.06	K	0	0.03	0.06	0.09
	α_{cr}	38°	42°	52°	55°
	Cn_{max}	1.50	1.86	2.06	2.13
0.09	K	0	0.04	0.08	0.12
	α_{cr}	38°	42°	54°	63°
	Cn_{max}	1.50	1.91	2.10	2.20

Table 4. Steady aerodynamic characteristic data of the experimental model with $\delta_f = -20°, \delta_v = 50°$ and -50°. (↑ : increasing, ↓ : decreasing)

δ_f	δ_v \ α	C_L 15°	C_L 65°	C_L 90°	C_{Lmax}	α_{cr}	C_d 15°	C_d α_{cr}	C_d 65°	C_d 90°
−20°	−50°	0.415	0.490	0.060	1.380	40°	0.070	1.100	1.070	1.130
	50°	0.675	0.345	0.010	1.230	35°	0.220	1.020	0.875	0.860
	Increment	+0.260 ↑	−0.145 ↓	−0.05 ↓	−0.150 ↓	−5° ↓	+0.150 ↑	−0.080 ↓	−0.195 ↓	−0.270 ↓

Table 5. Steady aerodynamic characteristic data of the experimental model with $\delta_v = -30°, \delta_f = 15°$ and -15°. (↑ : increasing, ↓: decreasing)

δ_v	δ_f \ α	C_L 15°	C_L 65	C_L 90°	C_{Lmax}	α_{cr}	C_d 15°	C_d α_{cr}	C_d 65°	C_d 90°
−30°	−15°	0.530	0.560	0.01	1.40	37°	0.09	1.09	1.10	1.11
	15°	0.600	0.510	0.00	1.23	35°	0.15	1.00	1.10	1.10
	Increment	+0.070 ↑	−0.050 ↓	−0.01 ↓	−0.170 ↓	−2° ↓	+0.06 ↑	−0.09 ↓	0	−0.01 ↓

Table 6. Data comparison of the model with flaps and the calibration delta-model

K	Parameter	C_{xmax}	α_{cr}	α_{ed}	α° Zone	Re no.
0	Present	1.65	36		0–90	1×10^6
	Ref. [9]	1.50	34		0–90	4.5×10^5
0.03	Present	1.86	40	19	0–40	1×10^6
	Ref. [9]	1.86	47	20	0–90	4.5×10^5
0.04	Present	2.01	45	24	20–60	1×10^6
	Ref. [9]	1.97	48	18	0–90	4.5×10^5
0.06	Present	2.1	50	22	20–60	1×10^6
	Ref. [9]	1.92	50	12	0–90	4.5×10^6

Figures

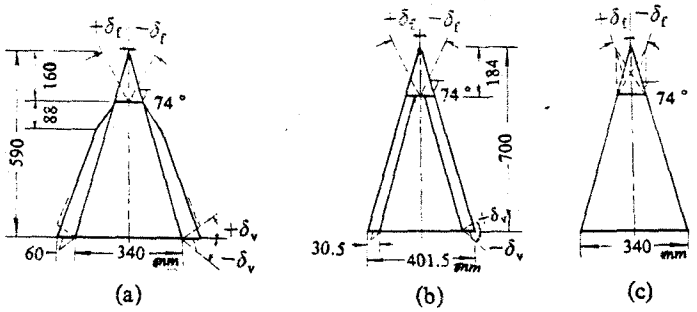

Fig.1 Planeforms of the experimental models
(a) Present Model (b) Previous Model (c) Delta-Wing

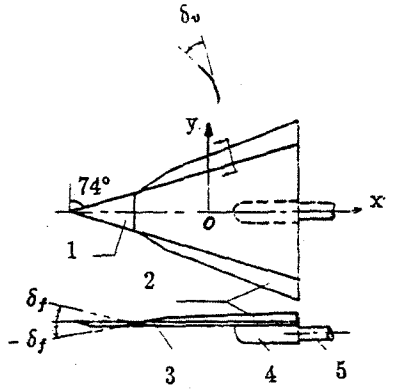

Fig.2 Coordinates and sketch of the sting-support
(1) apex flap (2) leading-edge vortex-flap (3) main wing (4) wing supporter (5) strain-gage balance and sting-support

(d) $\alpha=45°$, $\delta_v=30°$, $\delta_f=0°$ (c) $\alpha=30°$, $\delta_v=-30°$, $\delta_f=-15°$ (b) $\alpha=30°$, $\delta_v=30°$, $\delta_f=-15°$ (a) $\alpha=30°$, $\delta_v=30°$, $\delta_f=5°$

Fig.3 Water channel pictures showing the flow patterns around the model with various flap deflections

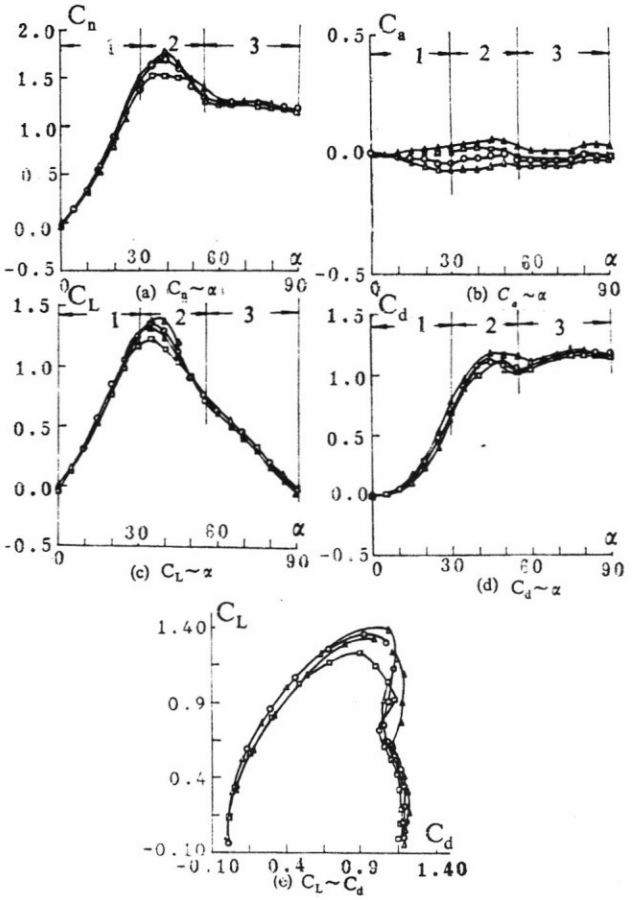

Fig.4 Experimental results showing the variation of Cn, Ca, CL, Cd and Cmz vs.α and Cl vs.Cd for the model with various flap deflections ($\delta_v = -30°$) in steady state $\delta_f=0°$-○- $\delta_f=15°$-□- $\delta_f=-15°$-△- Delta Wing -▲-

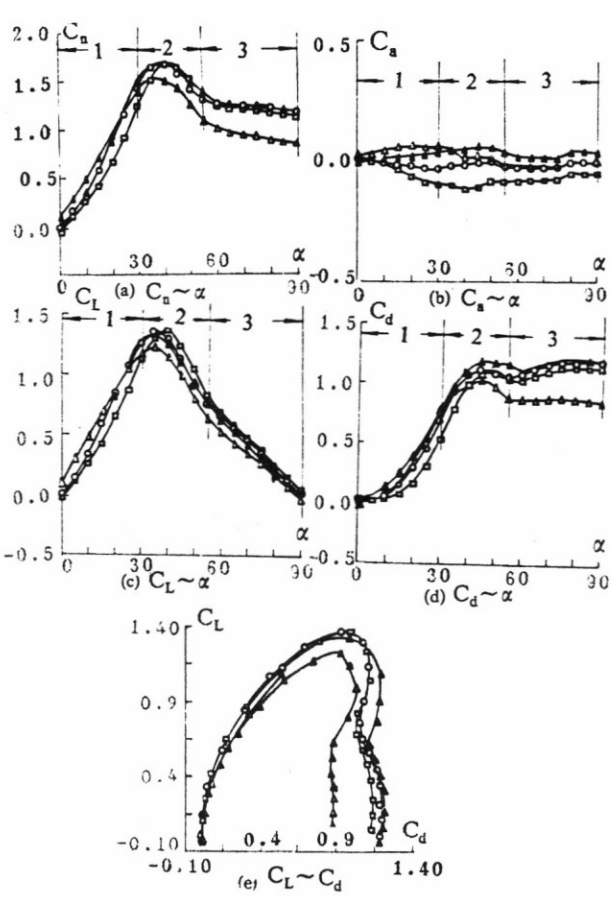

Fig.5 Experimental results showing the variation of Cn, Ca, CL, Cd and Cmz vs. α and Cl vs. Cd for the model with various flap deflections ($\delta_v = 50°$) in steady state $\delta_v=-30°$ $\delta_f=0°$ -○- $\delta_v=-50°$ $\delta_f=-20°$ -□- $\delta_v=50°$ $\delta_f=-20°$ -△- Delta Wing -▲-

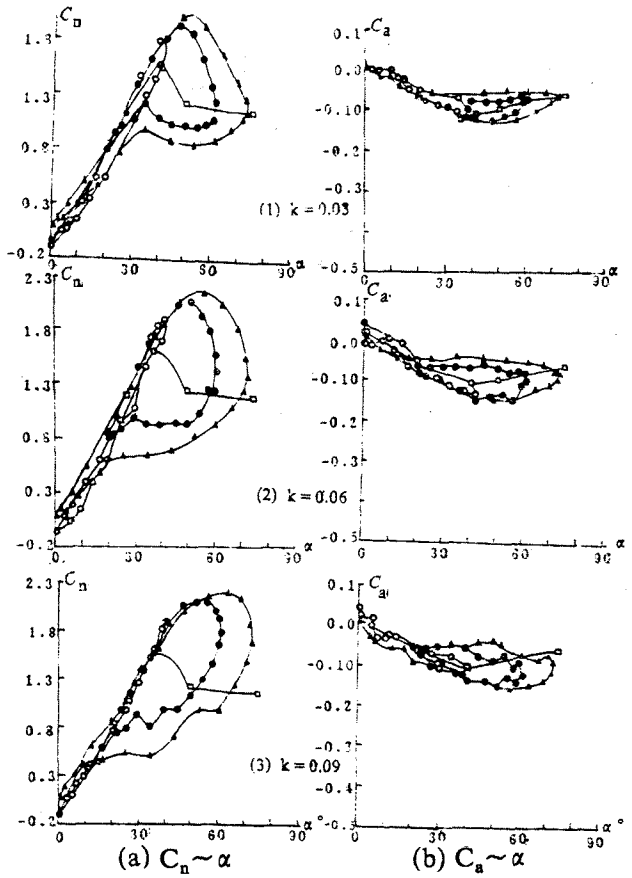

Fig.6 Experimental results showing the variation of Cn and Ca vs. α for the model pitching with various frequencies and amplitudes in unsteady state $\delta_v = -30°$

α	$0° \rightarrow 90°$	$0° \rightleftharpoons 40°$	$20° \rightleftharpoons 60°$	$0° \rightleftharpoons 73°$
$\delta_f = -15°$	steady -□-	-○-	-●-	-▲-

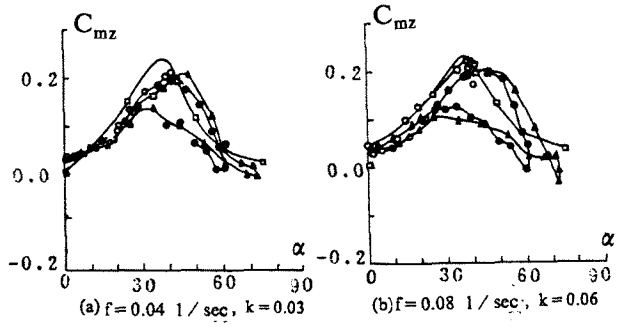

Fig.7 Experimental results showing the variation of Cmz vs. α for the model pitching with various frequencies and amplitudes in unsteady state

(a) K=0.02 -○- K=0.04 -●- K=0.06 -▲- steady-□-
(b) K=0.03 K=0.09 K=0.12

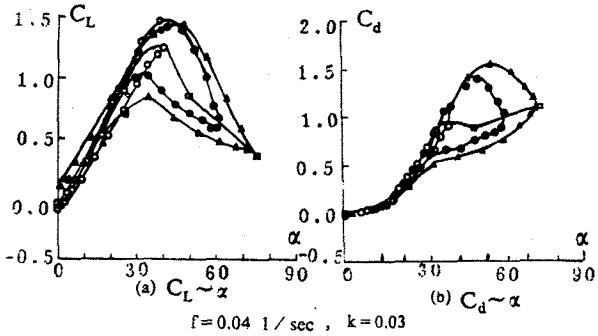

Fig.8 Experimental results showing the variation of CL and Cd vs. α for the model pitching with reduced frequency k=0.03 and various amplitudes in unsteady state

K=0.02 -○- K=0.04 -●- K=0.06 -▲- steady-□-

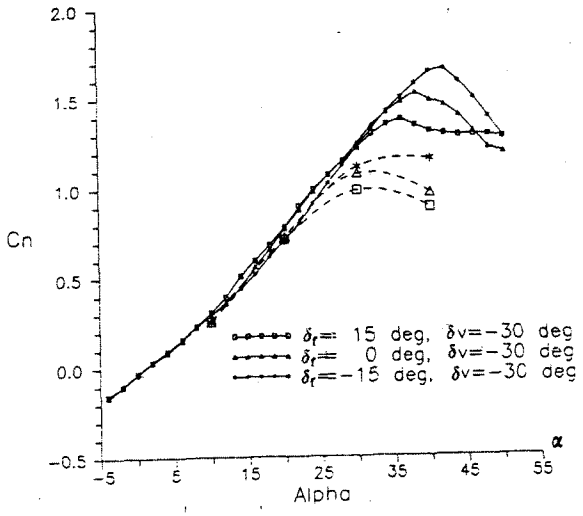

Figure 9 (a) normal force

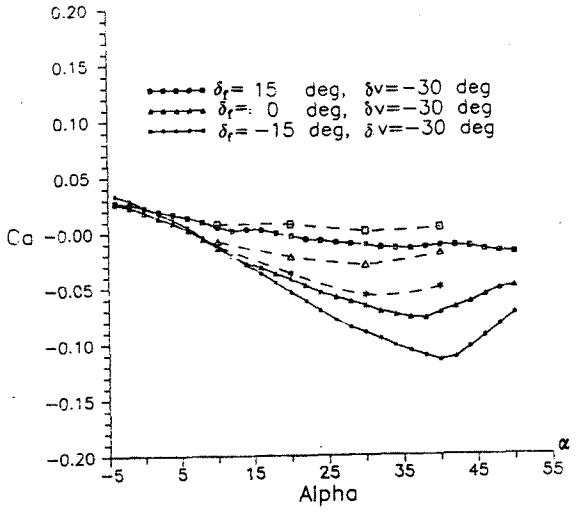

Figure 9 (b) axial force

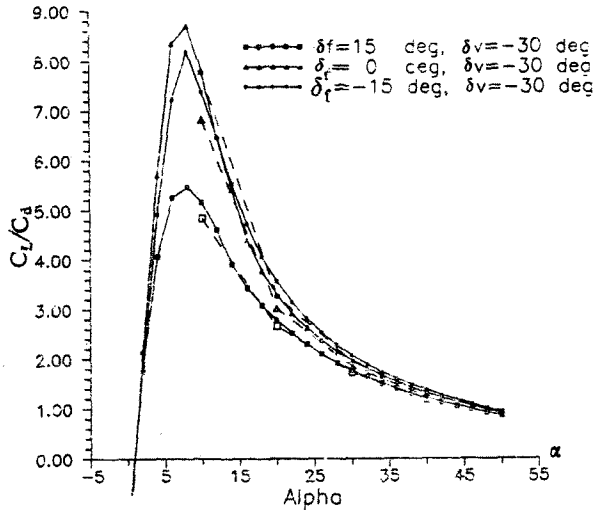

Figure 9(d) lift/drag ratio

Fig.9 Comparison of the aerodynamic characteristics between the experimental and computational results solid lines: experiment; dashed lines with larger symbols: computation.

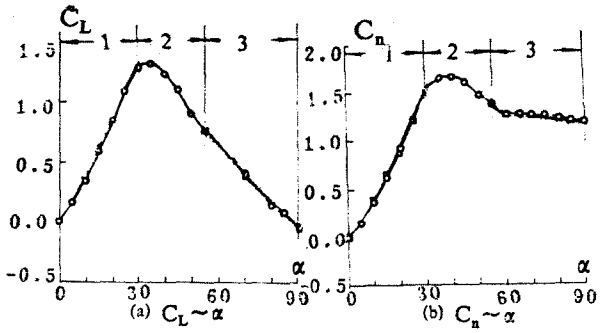

Fig.10 Aerodynamic characteristic Cl and Cd vs. α curves of the calibration delta-model